Data Repository Item

This is a supplementary text for the paper, "Fujioka et al., Australian dune fields initiated with Pliocene-Pleistocene global climatic shift", submitted to *Geology*, containing details of cosmogenic nuclide and optically stimulated luminescence (OSL) analyses, and of multistage dune formation model discussed in text.

1. Cosmogenic nuclide analysis

Sand samples were washed to discard dust, and then sieved to 250–500 μm size. Quartz was extracted and purified following the standard procedure (Kohl and Nishiizumi, 1992). The sieved materials were treated in aqua regia (1:1 of HCl: HNO_3) at 50°C for up to two weeks to remove iron oxides, which was essential because the sand grains used in this study were typically coated by haematite. Next, the residues were leached by 2% HF-HNO_3 solution in an ultrasonic bath at 60°C for at least 72 hours. This treatment removed residual clays and feldspars, and etched quartz grain surfaces to remove meteoric ^{10}Be and obtain ultra pure quartz with 60–120 ppm Al. Beryllium and aluminium were then extracted by ion exchange chromatography. The pure quartz aliquots were spiked with 0.5 mg of ^{9}Be and dissolved in HF and HNO_3 solution. The solutions were fumed with $HClO_4$ to remove Si. Iron was then removed on an anion exchange column, followed by separation of Be and Al on a cation exchange column. After coprecipitation of the hydroxides with AgO, the samples were baked at 800°C to convert them to intimate mixtures of the oxides and silver (BeO–Ag and Al_2O_3–Ag) (Stone et al., 2004), mixed with Nb powder (Be samples only) and packed into copper AMS target holders.

AMS measurements were performed at the 14UD pelletron accelerator facility in the Department of Nuclear Physics at the ANU (Fifield, 1999; Fifield et al., 2007). For ^{10}Be calibration, the NIST standard SRM4325 was employed with an assumed ^{10}Be/^{9}Be value of 3.00 x 10^{-11} (Middleton et al., 1993). This value has been widely used in the literature, and in particular most of the measurements on which the calibration of the production rate of ^{10}Be in quartz is based would have used it. It differs, however, from the NIST-certified value of 2.68 ± 0.14 x 10^{-11}. A recent re-evaluation of the ratio of this standard (Nishiizumi et al., 2007) indicates that the NIST value may in fact be correct. Nevertheless, we have opted to use the 3.00 x

10^{-11} value and a production rate of ^{10}Be in quartz at sea level and high latitude of 5.1 ± 0.3 atoms g^{-1} yr^{-1} (Stone, 2000), because the full implications of using a revised value for the standard are yet to be explored. For ^{26}Al calibration, a standard with $^{26}Al/^{27}Al$ of 4.11 x 10^{-11} that was prepared by Stephan Vogt at Purdue University was used. Values of ^{10}Be and ^{26}Al concentrations shown in Table 1 in text are relative to the standards.

Independently of the new measurement of the $^{10}Be/^{9}Be$ ratio of the NIST standard, Nishiizumi et al. (2007) also redetermined the ^{10}Be half-life, and proposed that it should be revised downwards from the commonly used value of 1.51 Ma to 1.36 Ma. The discrepancy between the two values is relatively large (~10%), which would affect our burial age and model calculations. For the simple burial ages of the dune base (mean of four samples, 1.12 Ma, in Table 1 in text) determined in the present work, the effect of adopting the shorter half-life would be to increase the burial age by 12% to 1.25 Ma. For the dune initiation age derived by multistage dune formation model (1.02 Ma, see text and below, for the model detail), the effect would be to increase the age by 10% to 1.12 Ma. However, such changes would not alter the conclusions of the present work.

2. OSL analysis

2.1. OSL measurements

Optical dating of 29 sediment samples was performed at the Australian National University using the optically stimulated luminescence (OSL) signal of quartz. Samples were collected in steel tubes using a truck-mounted drill rig. Quartz grains of either 125–180 or 180–212 μm were separated by wet sieving, etched with 40% HF for 100 min to remove the alpha-irradiated outer layer, separated from heavy minerals with sodium polytungstate (S.G. 2.68 g cm^{-3}), and sieved again to remove heavily etched grain fragments (Rhodes, 1988). All procedures were done under low-intensity red and orange light. OSL measurements used a single aliquot regenerative-dose (SAR) protocol (Murray and Wintle, 2000, 2003), and were made on Risø equipment using either a 150W halogen lamp filtered to provide 420–560 nm, or Nichia blue diodes with Schott GG420 filters giving a peak wavelength of 470 ± 20 nm. OSL signals were detected through Hoya U340 glass filters with 9235QA PMTs, at 125ºC for 50 sec. For each measurement, counts from the first 1 sec were used as

signal, and counts from the final 12 sec were scaled and subtracted as background. The preheat procedure was 10 sec at 260ºC before measurement of each natural and regenerated OSL, and 10 sec at 220ºC before each test dose measurement. High OSL sensitivity, good recycling (typically within 2% of unity) and low thermal transfer values (below 1% of the natural OSL signal) were observed, and both measured TL (thermoluminescence) and LM-OSL (linear modulation OSL) comprised signal components typical of quartz Singarayer and Bailey (2004). Figures DR1 and DR2 present typical OSL decay and growth curve data for aliquots of two samples.

Dose rates were calculated using concentrations of U, Th and K determined by neutron activation analysis (NAA) at Bequerel laboratories, Lucas Heights, NSW, Australia and ICP-MS/ICP-OES at Genalysis, Perth, WA, Australia, with the dose rate conversion factors of Ademiec and Aitken (1998) and beta attenuation values of Mejdahl (1979). Cosmic dose rates were estimated using the equations of Prescott and Hutton (1994) using present day burial depths, and a uniform water content of 5 ± 2 %, based on measured *in situ* values, was used following the equations in Aitken (1985). Comparison of ^{238}U from the NAA and ICPMS measurements with ^{214}Bi from *in situ* gamma measurements indicates no significant U-series disequilibrium. High resolution Ge gamma spectrometry confirmed the absence of any significant U-series disequilibrium.

2.2. OSL dating results

Table DR1 presents OSL dating results for 29 samples, comprising sample field codes, including sample depth, laboratory codes, K, Th and U concentrations, equivalent dose values, total dose rates and age estimate in ka (thousand years). For saturated samples, we used the highest administered regenerative-dose value, so these values are minimum age estimates; these equivalent dose and age results are indicated in the table. All uncertainties shown are one-sigma values. Some samples displayed variation in equivalent dose value between aliquots, indicating a mixed dose population (Figure DR3). The age estimates presented in Table DR1 and in Figure 2 within text are based on the lowermost grouping of dose values. This implies an interpretation of incomplete OSL signal zeroing at deposition as responsible for the mixed dose population, though for several samples, the introduction of younger grains from above by bioturbation is an alternative explanation. This point is discussed within text for samples lying below paleosols P1 and P2, and inspection of the dose

distributions of K0200, K0209, K0220 and K0234 confirms that these samples may have been subject to grain mixing by bioturbation, and that their depositional ages are probably higher than those presented. The degree to which dose estimates may be determined using multiple-grain SAR data for samples which have experienced mixing is discussed in detail by Rhodes (2007).

These samples have relatively high dose rates, caused by the regionally high concentrations of K, Th and U in the dunes, causing saturation to limit the luminescence dating range at lower ages than for areas with lower dose rates (Huntley and Prescott, 2001). These relatively high dose rates mean that the age estimates are relatively unaffected by variations in cosmic dose rate caused by changes in overburden thickness. We have therefore not modelled the effects of changes in burial depth on the OSL age estimates during periods of dune accumulation and subsequent denudation.

The OSL dating methods and error propagation used here are similar to those applied by Rhodes et al. (2003) who demonstrated good agreement between AMS ^{14}C dating of burnt seeds with OSL dates of Scottish archaeological sediments. No systematic error was observed for these OSL age estimates of around 2000 years before present, with uncertainties in the region of ± 2 to 4 % at one sigma. Rhodes et al. (2006) presented significantly older OSL age estimates for shallow marine and eolian sands from Morocco, in apparent agreement with U-series age control at around 400 ka. These carbonate-rich sandy sediments have low dose rates. Uncertainty values on both techniques are large, but no indication of systematic error is provided by this comparison. Murray and Funder (2003) dated Eemian (last interglacial) marine deposits in Denmark, and found a small systematic age underestimation, comparable to the size of the overall age uncertainties.

3. Multistage dune formation model

The mechanism of linear dune formation has long been debated (Mabbutt, 1977; Tsoar et al., 2004), but a recent study found no downwind decrease in OSL ages of sand grains, supporting a wind-rift model where sand is rifted laterally onto dune-ridges from nearby swales with no significant downwind elongation (Hollands et al., 2006). We adopt this model and assume that sand is recycled between swales and ridges. We assume four cyclic episodes of dune building alternating with pedogenesis and partial deflation, as we recognised four dune units separated by three paleosol

horizons. Dune accretion above the preceding paleosol is assumed to be the same in each cycle: each dune crest is assumed to have stood 5 m above its prior paleosol, flanks at the position of the drill holes being 3 m above their prior paleosols. However, it turned out that the final estimate of the dune-field age is not sensitive to the extent of accretion. During the pedogenesis phase following dune building, the dune surface is assumed to be deflated to the paleosol capping the dune sand of that cycle. Table DR2 gives the sequence of burial depths for each sample.

The fractional duration of the pedogenesis phase within each cycle is assumed to be the same in each cycle, and is represented by parameter α in the model. The two most recent cycles are assigned to the last and penultimate glacial cycles, with each given a nominal duration of 100 ka on the basis of their OSL ages, while the timing of the earlier cycles is unknown. While it is likely that these earlier cycles are themselves composites of several 100 ka cycles, these are not stratigraphically resolved. Accordingly, they are treated as two simple cycles and are assumed to have been of equal duration (t_c). Finally, the stacked paleosols suggest the addition of externally-sourced sand during evolution of the dune field. Accordingly, the model includes two options: either zero addition, or a doubling of the sand volume in three steps, following formation of paleosol P3, where it turned out that effects from the selection of these options are minimal to the final estimate of dune initiation timing.

We assume that the initial dune field was swept up on a prior alluvial plain of well-mixed sand, with uniform amounts of cosmogenic nuclides, $N_i(0)$ (i = ^{10}Be, ^{26}Al). Hence, we seek to evaluate the unknowns: t_c, α and $N_i(0)$, using measured ^{10}Be and ^{26}Al from our sample ensemble. This is done by a simple inverse method. Initial values are assigned to the unknown variables, and expected values of $N_i(t)$ (for both ^{10}Be and ^{26}Al) are calculated with equation 1 (in text) in a series of steps, using the sample-specific depth histories shown in Table DR2. The calculation includes cosmogenic nuclide production by both secondary cosmic ray neutrons and muons. Differences between expected and observed $N_i(t)$ are summed to give a misfit measure for the ensemble of samples (equation S1, below), and the unknowns are varied until misfit is minimised (note: a similar approach has undertaken to evaluate paleosol ages in Pliocene-Pleistocene glacial deposits in Balco et al. (2005)).

Two further details of the calculation are noted. We use steady-state erosion rate ε at the sediment source as a variable (see equation 2 in text), because this

determines the initial nuclide concentrations of both ^{10}Be and ^{26}Al and reduces two unknown of $N_i(0)$ (for both ^{10}Be and ^{26}Al) to a single unknown. Note that we assumed relatively short transport of sand grains from the source to floodplain and short residence time in the floodplain, i.e., ~10^4–10^5 yr, where nuclide production and/or loss by decay during these periods is negligible. This assumption may be justified as the simple model burial ages shown in Table 1 (in text) have a clear discrimination between dune units, where such discrimination would not be seen if transport or residence time in the floodplain is considerably longer than burial time in dunes.

The misfit function is based on the difference between expected and observed values of both ^{10}Be and the ^{26}Al/^{10}Be ratio (these are the axes of the "banana-plot" diagram that is widely used for assessing departures from steady-state erosion (Lal, 1991)). The misfit measure M for a single sample is:

$$M = \left[\frac{{}^{10}Be_o - {}^{10}Be_m}{{}^{10}Be_o}\right]^2 + \left[\frac{\left({}^{26}Al/{}^{10}Be\right)_o - \left({}^{26}Al/{}^{10}Be\right)_m}{\left({}^{26}Al/{}^{10}Be\right)_o}\right]^2 \quad \text{(S1)}$$

where subscripts o and m denote observed and model values, respectively. M is summed over all samples to give the total misfit.

Finally, values for the fixed parameters used in the model calculation are the same as those noted in Table 1. To be added are the production rates at the sampling site of 4.3 and 26.3 atoms g^{-1} yr^{-1} for ^{10}Be and ^{26}Al, respectively, which is scaled from the commonly-used values (Lal, 1991; Stone, 2000), and the sand density of 1.7 g cm^{-3}.

References

Ademiec, G., and Aitken, M.J., 1998, Dose-rate conversion factors: update: Ancient TL, v. 16, p. 37-50.

Aitken, M.J., 1985, Thermoluminescence Dating: London, Academic Press.

Balco, G., Stone, J.O., and Mason, J.A., 2005, Numerical ages for Plio-Pleistocene glacial sediment sequences by ^{26}A l/^{10}Be dating of quartz in buried paleosols: Earth and Planetary Science Letters, v. 232, p. 179-191.

Fifield, L.K., 1999, Accelerator mass spectrometry and its applications: Reports on Progress in Physics, v. 62, p. 1223-1274.

Fifield, L.K., Tims, S.G., Gladkis, L.G., and Morton, C.R., 2007, ^{26}Al measurements with ^{10}Be counting statistics: Nuclear Instruments and Methods in Physics Research B, v. 259, p. 178-183.

Hollands, C.B., Nanson, G.C., Jones, B.G., Bristow, C.S., Price, D.M., and Pietsch, T.J., 2006, Aeolian-fluvial interaction: evidence for Late Quaternary channel change and wind-rift linear dune formation in the northwestern Simpson Desert, Australia: Quaternary Science Reviews, v. 25, p. 142-162.

Huntley, D.J., and Prescott, J.R., 2001, Improved methodology and new thermoluminescence ages for the dune sequence in south-east South Australia: Quaternary Science Reviews, v. 20, p. 687-699.

Kohl, C.P., and Nishiizumi, K., 1992, Chemical isolation of quartz for measurements of *in situ* produced cosmogenic nuclides: Geochimica et Cosmochimica Acta, v. 56, p. 3583-3587.

Lal, D., 1991, Cosmic ray labeling of erosion surfaces: *in situ* nuclide production rates and erosion models: Earth and Planetary Science Letters, v. 104, p. 424-439.

Mabbutt, J.A., 1977, An Introduction to Systematic Geomorphology, 2: Desert Landforms: Canberra, Australian National University Press.

Mejdahl, V., 1979, Thermoluminescence dating: beta dose attenuation in quartz grains: Archaeometry, v. 21, p. 61-73.

Middleton, R., Brown, L., Dezfouly-Arjomandy, B., and Klein, J., 1993, On ^{10}Be standards and the half-life of ^{10}Be: Nuclear Instruments and Methods in Physics Research B, v. 82, p. 399-403.

Murray, A.S., and Funder, S., 2003, Optically stimulated luminescence dating of a Danish Eemian coastal marine deposit: a test of accuracy: Quaternary Science Reviews, v. 22, p. 1177-1183.

Murray, A.S., and Wintle, A.G., 2000, Luminescence dating of quartz using an improved single-aliquot regenerative-dose protocol: Radiation Measurements, v. 32, p. 57-73.

—, 2003, The single-aliquot regenerative-dose protocol: potential for improvements in reliability: Radiation Measurements, v. 37, p. 377-381.

Nishiizumi, K., Imanura, M., Caffee, M.W., Southon, J.R., Finkel, R.C., and McAninch, J., 2007, Absolute calibration of ^{10}Be AMS standards: Nuclear Instruments and Methods in Physics Research B, v. 258, p. 403-413.

Prescott, J.R., and Hutton, J.T., 1994, Cosmic ray contributions to dose rates for luminescence and ESR dating: large depths and long term time variations: Radiation Measurements, v. 23, p. 497-500.

Rhodes, E.J., 1988, Methodological considerations in the optical dating of quartz: Quaternary Science Reviews, v. 7, p. 395-400.

—, 2007, Quartz single grain OSL sensitivity distributions: implications for multiple grain single aliquot dating: Geochronometria, v. 26, p. 19-29.

Rhodes, E.J., Bronk Ramsey, C., Outram, Z., Batt, C., Willis, L., Dockrill, S., and Bond, J., 2003, Bayesian methods applied to the interpretation of multiple OSL dates: high precision sediment age estimates from Old Scatness Broch excavations, Shetland Isles: Quaternary Science Reviews, v. 22, p. 1231-1244.

Rhodes, E.J., Singarayer, J.S., Raynal, J.-P., Westaway, K.E., and Sbihi-Alaoui, F.Z., 2006, New age estimates for the Palaeolithic assemblages and Pleistocene succession of Casablanca, Morocco: Quaternary Science Reviews, v. 25, p. 2569-2585.

Singarayer, J.S., and Bailey, R.M., 2004, Component-resolved bleaching spectra of quartz optically stimulated luminescence: preliminary results and implications for dating: Radiation Measurements, v. 38, p. 111-118.

Stone, J.O., 2000, Air pressure and cosmogenic isotope production: Journal of Geophysical Research, v. 105, p. 23753-23759.

Stone, J.O., Fifield, L.K., Beer, J., Vonmoos, M., Obrist, C., Grajcar, M., Kubik, P., Muscheler, R., Finkel, R., and Caffee, M., 2004, Co-precipitated silver-metal oxide aggregates for accelerator mass spectrometry of ^{10}Be and ^{26}Al: Nuclear Instruments and Methods in Physics Research B, v. 223-224, p. 272-277.

Tsoar, H., Blumberg, D.G., and Stoler, Y., 2004, Elongation and migration of sand dunes: Geomorphology, v. 57, p. 293-302.

Data Repository Item

Table DR1. Summary of OSL measurements

Field code including depth (m)	Laboratory code	K conc. (% K)	Th conc. (ppm Th)	U conc. (ppm U)	Equivalent dose (Gy)		1 sigma uncertainty	Total dose rate (mGy/a)		1 sigma uncertainty	Age (ka)		1 sigma uncertainty
S02/3.0	K0198	1.3	5.4	1.1	30	±	2	1.92	±	0.10	16	±	1
S02/4.0	K0199	1.3	4.6	1.5	137	±	5	1.98	±	0.10	69	±	4
S02/5.0	K0200	1.3	4.9	0.9	160	±	10	1.80	±	0.10	89	±	8
S02/6.0	K0201	1.3	7.1	1.5	>318	±	11	2.07	±	0.11	>154	±	9
S02/7.0	K0202	1.2	4.4	0.8	>300	±	31	1.66	±	0.09	>180	±	21
S02/8.0	K0203	1.4	4.4	0.9	>300	±	31	1.83	±	0.10	>164	±	19
S02/9.0	K0204	1.4	4.8	1.3	>1155	±	301	1.97	±	0.11	>587	±	156
S02/10.0	K0205	1.4	5.5	1.4	>691	±	88	2.05	±	0.11	>338	±	47
S02/11.5	K0206	1.4	6.0	1.3	>350	±	28	1.99	±	0.11	>176	±	17
S03/2.9	K0207	1.1	3.2	1.2	23	±	1	1.63	±	0.09	14	±	1
S03/4.4	K0208	1.0	3.3	1.4	136	±	7	1.55	±	0.08	88	±	6
S03/5.9	K0209	1.2	3.7	1.7	144	±	7	1.81	±	0.09	79	±	6
S03/7.4	K0210	0.9	4.9	0.6	>250	±	25	1.37	±	0.07	>183	±	21
S03/8.9	K0211	1.3	5.1	1.7	>243	±	9	1.96	±	0.10	>124	±	8
S04/2.0	K0212	1.3	7.1	1.2	155	±	9	2.11	±	0.11	73	±	6
S04/3.0	K0213	1.2	5.6	2.2	147	±	7	2.13	±	0.10	69	±	5
S04/4.0	K0214	1.4	4.8	1.6	>250	±	25	2.08	±	0.11	>120	±	14
S04/5.0	K0215	1.1	3.8	0.4	>362	±	34	1.51	±	0.09	>240	±	27
S04/6.0	K0216	1.2	5.0	0.6	>381	±	26	1.62	±	0.09	>234	±	20
S04/7.0	K0217	1.2	4.3	0.5	>341	±	23	1.56	±	0.09	>219	±	19
S04/8.0	K0218	1.3	4.5	1.8	>373	±	21	1.95	±	0.10	>191	±	15
S05/2.0	K0219	0.9	3.6	0.8	62	±	3	1.41	±	0.07	44	±	3
S05/3.0	K0220	1.3	5.1	0.6	178	±	13	1.78	±	0.10	100	±	9
S05/4.0	K0221	1.1	4.2	0.5	291	±	41	1.54	±	0.09	188	±	29
S05/5.0	K0222	1.2	5.1	0.5	283	±	41	1.63	±	0.09	174	±	27
S05/6.0	K0223	1.5	5.4	2.0	>261	±	13	2.31	±	0.12	>113	±	8
S08/2.0	K0232	1.1	4.1	1.5	97	±	6	1.80	±	0.09	54	±	4
S08/3.0	K0233	1.0	4.2	0.5	190	±	14	1.44	±	0.08	132	±	12
S08/4.0	K0234	1.0	4.0	0.5	197	±	6	1.36	±	0.07	145	±	9

Table DR2. Sequential depth profiles used for the multi stage dune formation model

Sample	Dune and drill hole position*	Depth † (m)						
		Cycle 1		Cycle 2		Cycle 3		Cycle 4
		d	p	d	p	d	p	d
Between surface and P1								
S3/3.0	CFS-c	*1.1*	*0.4*	*1.1*	*0.4*	*1.1*	*0.4*	3.2
S3/4.5	CFS-c	*1.1*	*0.4*	*1.1*	*0.4*	*1.1*	*0.4*	4.8
Between P2 and P3								
S2/11.0	MS-c	*1.1*	*0.4*	4.1	4.0	9.0	6.7	11.1
S4/6.0	MS-e	*1.1*	*0.4*	1.3	0.6	3.6	1.0	6.3
S4/7.0	MS-e	*1.1*	*0.4*	2.2	1.5	4.5	2.0	7.2
S5/6.0	MS-w	*1.1*	*0.4*	2.9	0.5	3.5	3.8	6.2
S8/4.0	CFS-w	*1.1*	*0.4*	2.5	0.9	3.9	1.8	4.2
Between P3 and substrate								
S4/8.0	MS-e	4.1	0.1	3.1	2.4	5.4	2.9	8.1
S5/7.0	MS-w	2.8	0.8	3.8	1.4	4.4	4.7	7.1
S3/8.7	CFS-c	1.7	0.7	5.7	2.0	7.0	3.3	8.8
S8/4.7	CFS-w	0.7	0.1	3.1	1.5	4.5	2.4	4.8

Note: Depth profiles are set as follows. Sample depths during the first dune-building phase (Cycle 1-d) are set with an assumed dune profile, 5 m at crest and 3 m at flank, taking the sample positions relative to dune base into account. Depths during pedogenesis phase (Cycles 1-p, 2-p and 3-p) are taken as observed sample depths below palaeosols P3, P2 and P1, respectively. Depths at subsequent dune-building phases (Cycles 2-d and 3-d) are calculated by adding 5 m for crest samples and 3 m for flank samples to their depths at the previous stages, respectively. Present sample depths are assigned for depths at Cycle 4-d. For top- (between surface and P1) and middle-stratigraphic-unit (between P2 and P3) samples, we assume that quartz grains are recycled between dune ridges and swales during earlier dune cycles until they are covered by palaeosols (cf. Fig. 3 in the main text). Average sample depths 1.1 and 0.4 m (italics) are estimated assuming average sand thicknesses of 3.0 m at dune ridges during dune building and 1.0 m at swale during pedogenesis phases, taking exponential depth-attenuation of cosmic ray neutrons and muons into account.

*Abbreviations follow as in Table 1 in the main text.

†Abbreviations "d" and "p" denote dune-building and pedogenesis phases in each cycle.

Data Repository Item

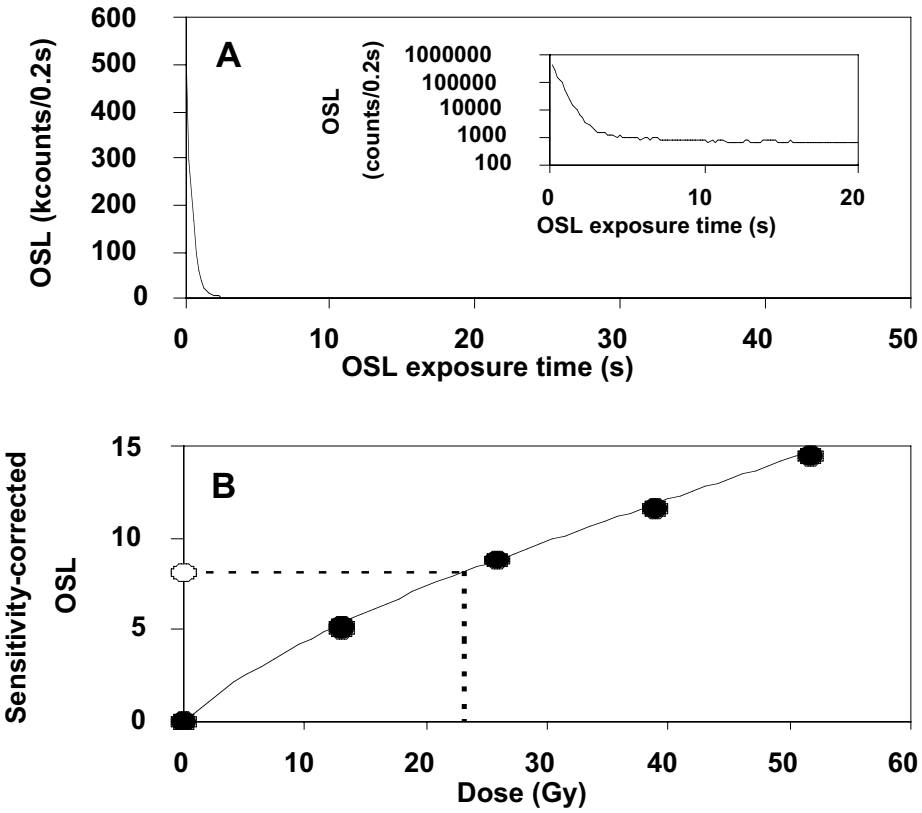

FigureDR1. (A) OSL decay of an aliquot of sample K207. Note y-axis scale is counts per 0.2 sec. Inset shows same data plotted for the first 20 sec on a logarithmic y-axis. (B) Growth curve of the same aliquot, plotting sensitivity-corrected OSL as a function of regenerative laboratory beta dose in Gy (solid symbols). The data are fitted using an exponential-plus-linear function (solid line). The sensitivity-corrected natural OSL intensity is indicated by the open symbol, and the dotted lines indicate the equivalent dose determination.

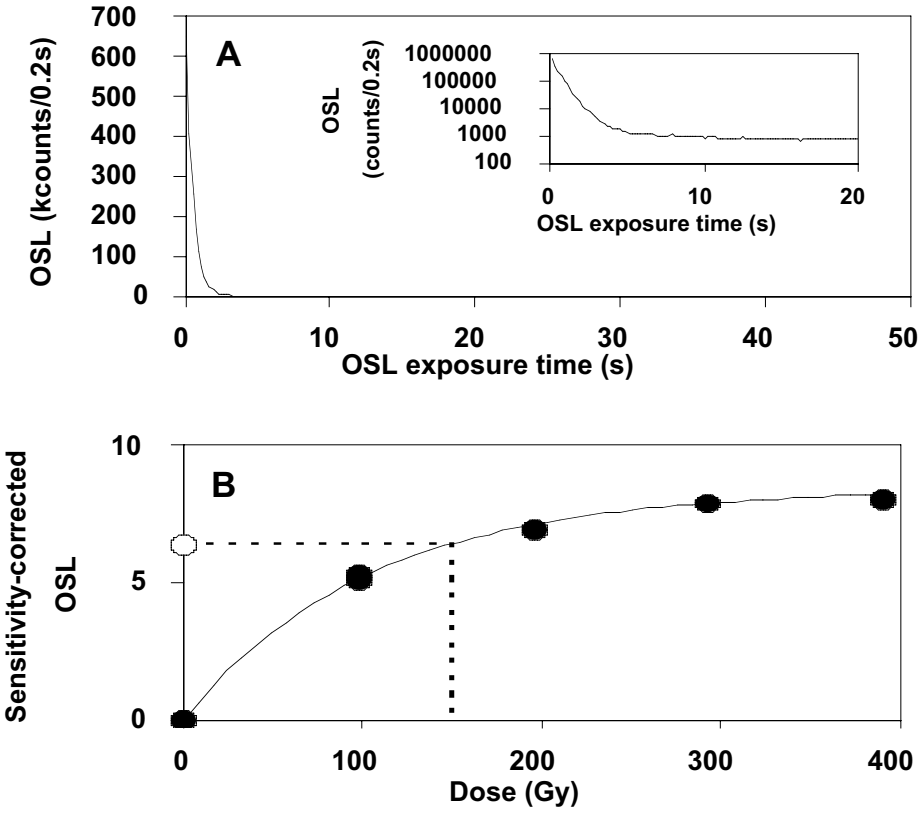

FigureDR2. (A) OSL decay of an aliquot of sample K220. Note y-axis scale is counts per 0.2 sec. Inset shows same data plotted for the first 20 sec on a logarithmic y-axis. (B) Growth curve of the same aliquot, plotting sensitivity-corrected OSL as a function of regenerative laboratory beta dose in Gy (solid symbols). The data are fitted using an exponential-plus-linear function (solid line). The sensitivity-corrected natural OSL intensity is indicated by the open symbol, and the dotted lines indicate the equivalent dose determination.

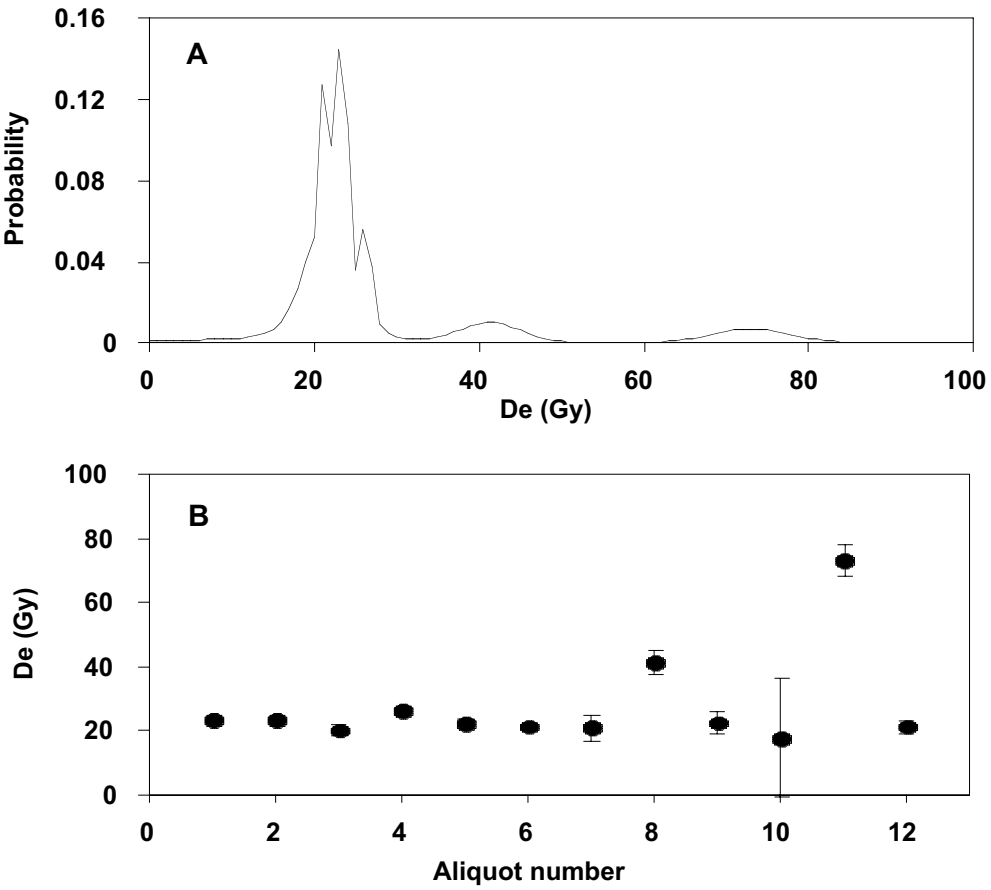

FigureDR3. Equivalent dose distribution for 12 aliquots of sample K207 plotted in two ways, as (A), a pdf plot representing the normalized sum of the 12 individual Gaussian distributions, and (B), the 12 D_e values in Gy, each with its associated one-sigma uncertainty. Some variation in D_e values is observed for this sample, specifically two aliquots which give significantly higher values, presumably caused by incomplete zeroing of the OSL signal at the time of deposition. Aliquots displaying significantly higher dose values were omitted from the age calculations.